ACS APPLIED MATERIALS & INTERFACES

Research Article

www.acsami.org

Synthesis of Hierarchical Three-Dimensional Vanadium Oxide Microstructures as High-Capacity Cathode Materials for Lithium-Ion Batteries

Anqiang Pan,[†] Hao Bin Wu,[†] Le Yu,[†] Ting Zhu,[†] and Xiong Wen (David) Lou*[,†]

[†]School of Chemical and Biomedical Engineering, Nanyang Technological University, 70 Nanyang Drive, Singapore 637457

ABSTRACT: Hierarchical three-dimensional (3D) vanadium oxide microstructures, including urchin-like microflowers, nanohorn-structured microspheres, nanosheet-assembled microflowers, and nanosheets bundles, are successfully synthesized by a versatile template-free solvothermal method. It is found that the concentration of the precursor (VOC_2O_4) solution has a significant effect on the morphologies of the products. As an example, the time-dependent phase and morphology evolution for the urchin-like vanadium oxide microflowers has been investigated in detail. Urchin-like VO_2 microflowers can be self-assembled within 2 h without using any surfactants. After calcination, the VO_2 microflowers can be easily transformed to urchin-like V_2O_5 microstructures. The as-obtained V_2O_5 microflowers are highly porous with a specific surface area of 33.64 $m^2\ g^{-1}$. When evaluated as a cathode material for lithium-ion batteries, the V_2O_5 sample delivers very high specific discharge capacity of 267 mA h g^{-1} at a current density of 300 mA g^{-1}. Further, it also exhibits improved cycling stability. The excellent electrochemical performance is attributed to multiple advantageous structural features, including the nanosized building blocks, high porosity, and the 3D hierarchical microstructures.

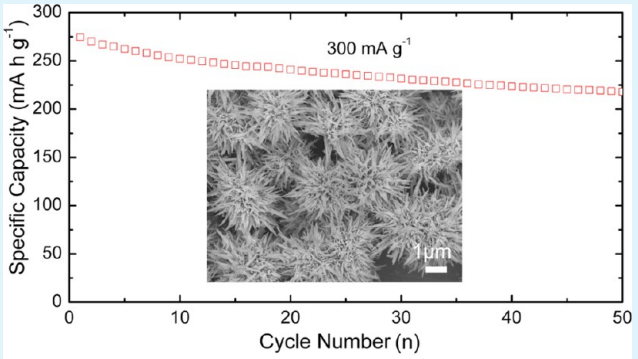

KEYWORDS: *vanadium oxide, V_2O_5, VO_2, cathode, lithium-ion batteries*

INTRODUCTION

Energy conversion and storage have unquestionably been one of the top concerns because of the fast depletion of fossil fuels and environmental problems, such as air pollution and global warming. More environmentally benign and sustainable energy storage systems are desired as future power sources.[1−3] Lithium-ion batteries (LIBs) are considered to be the most promising energy storage systems for consumer electronics, hybrid electric vehicles, and electric vehicles (EV) because of their high power output, long cycle life, and high energy density.[1,4] To meet some of the requirements, however, new electrode materials with higher lithium storage capacity are urgently needed to produce next-generation high-performance LIBs.[5−7]

Vanadium pentoxide (V_2O_5) has been extensively studied in diverse fields including LIBs,[8−10] catalysis,[11] sensors,[12] electrochromic devices,[13] and more recently in supercapacitors[14−16] because of the ease to accommodate molecules or ions into its layered structure. As a cathode material for LIBs, V_2O_5 can deliver a theoretical capacity of 440 mA h g^{-1} based on intercalation of three Li^+ ions,[17,18] which is about twice higher than that of $LiCoO_2$ (140 mA h g^{-1})[19] and $LiFePO_4$ (170 mA h g^{-1}).[20] However, the development of V_2O_5 electrodes in rechargeable lithium batteries has been limited by its poor structural stability,[21] low electronic conductivity[22] and slow electrochemical kinetics.[23] Because of the high surface area and reduced Li^+ ion diffusion distance, nanostructured vanadium oxides have been widely explored to enhance the electrochemical kinetics. Low-dimensional vanadium oxide structures, such as nanoparticles,[24] nanorods,[25] nanowires,[26] nanotubes,[27] and nanobelts,[28] have been successfully fabricated by a variety of methods and the rate capability is indeed greatly improved.[10,27] Nevertheless, it still remains as a big challenge to obtain a long-term stability during subsequent lithium insertion/extraction processes.[29] The capacity fading is always observed in low-dimensional nanosized materials for LIBs because it is easy for nanoparticles to agglomerate due to the very high surface area and surface energy.[5,6,30] 3D hierarchical nanostructures have attracted much attention as electrode materials for LIBs because the micro/nanostructures are believed to have better ability to suppress agglomeration, thus leading to improved capacity retention.[5,31,32]

It is generally known that the rate capability of LIBs is limited by solid-state Li^+ ion diffusion in the electrodes. Hence a highly porous 3D structure is advantageous in enhancing the rate capability and cycling stability.[33] Up until now, many strategies, including electrodeposition,[33] electrostatic spray deposition,[32] self-assembly,[34,35] and capillary-induced filling,[29] have been employed to synthesize 3D vanadium oxide porous structures. Self-assembly is believed to be one of the most facile routes to

Received: April 10, 2012
Accepted: July 18, 2012
Published: July 18, 2012

   dx.doi.org/10.1021/am3012593 | *ACS Appl. Mater. Interfaces* 2012, 4, 3874−3879

synthesize 3D nanostructures, in which well-defined aggregates are formed spontaneously.[36] It is therefore very attractive to develop facile and reliable synthesis methods for hierarchically self-assembled architectures with designed chemical components and controlled morphologies, which strongly determine the properties of nanomaterials.[34] For example, V_2O_5 hollow microspheres self-assembled from nanorods have been synthesized by Cao et al.,[34] in the presence of poly(vinylpyrrolidone) (PVP) in ethylene glycol. Urchin-like vanadium oxide nanostructures were also synthesized by treating an ethanolic solution of vanadium triisopropoxide and alkylamine hexadecylamine for 7 days.[35] However, the used vanadium organic salt precursor is very expensive and the synthesis is quite time-consuming. Also, the introduction of surfactants/polymers will inevitably increase the complexity of the synthesis. Therefore, it is of great interest to develop a template-free, cost-effective, and fast self-assembly process for preparation of 3D vanadium oxide nano/microstructures.

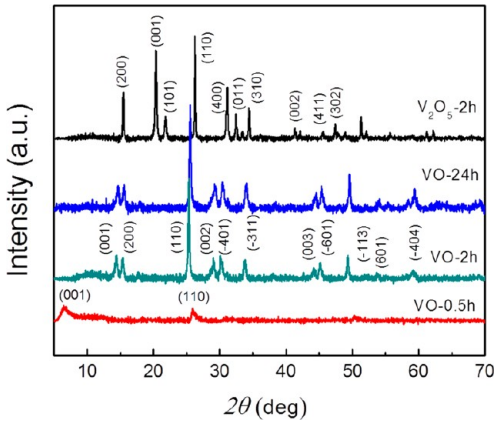

Figure 1. XRD patterns of three solvothermally prepared samples (VO-0.5 h, VO-2 h and VO-24 h) and the V_2O_5-2 h sample prepared by calcining VO-2 h in air at 350 °C for 2 h.

Herein, we report a facile solvothermal method to synthesize hierarchical vanadium oxide with various nano/microstructures by simply varying the concentration of the precursor (VOC_2O_4) solution. The vanadium oxide microstructures can be quickly synthesized within 2 h and the as-prepared urchin-like microflowers are highly porous. The vanadium oxide microflowers are easily transformed to V_2O_5 microflowers *via* calcination at 350 °C in air, without losing the pristine morphology. The electrochemical measurements of V_2O_5 nano/microflowers electrodes suggest excellent rate capability and cycling stability.

EXPERIMENTAL SECTION

Materials Synthesis. In a typical synthesis, V_2O_5 (1.2 g) and $H_2C_2O_4{\cdot}2H_2O$ in a molar ratio of 1:3 were dissolved in 40 mL of

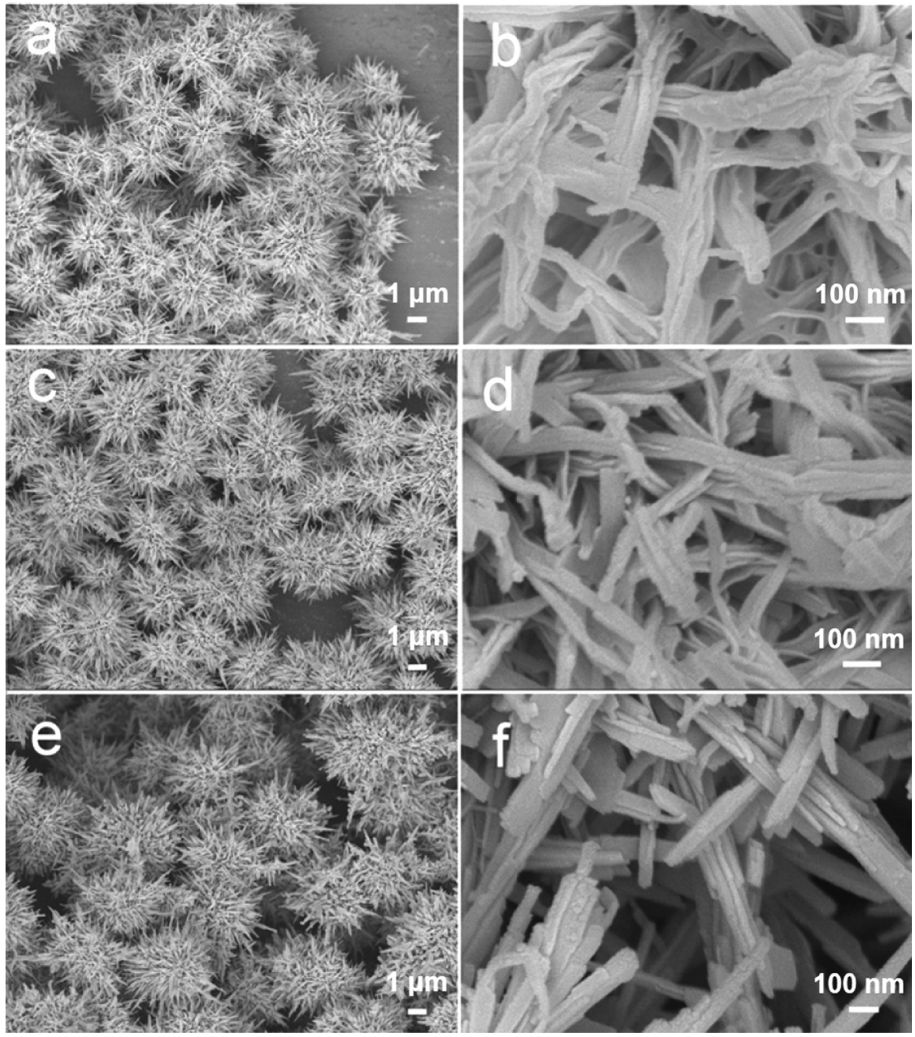

Figure 2. FESEM images of three solvothermally prepared vanadium oxide samples: (a, b) VO-0.5 h, (c, d) VO-2 h, and (e, f) VO-24 h.

dx.doi.org/10.1021/am3012593 | ACS Appl. Mater. Interfaces 2012, 4, 3874−3879

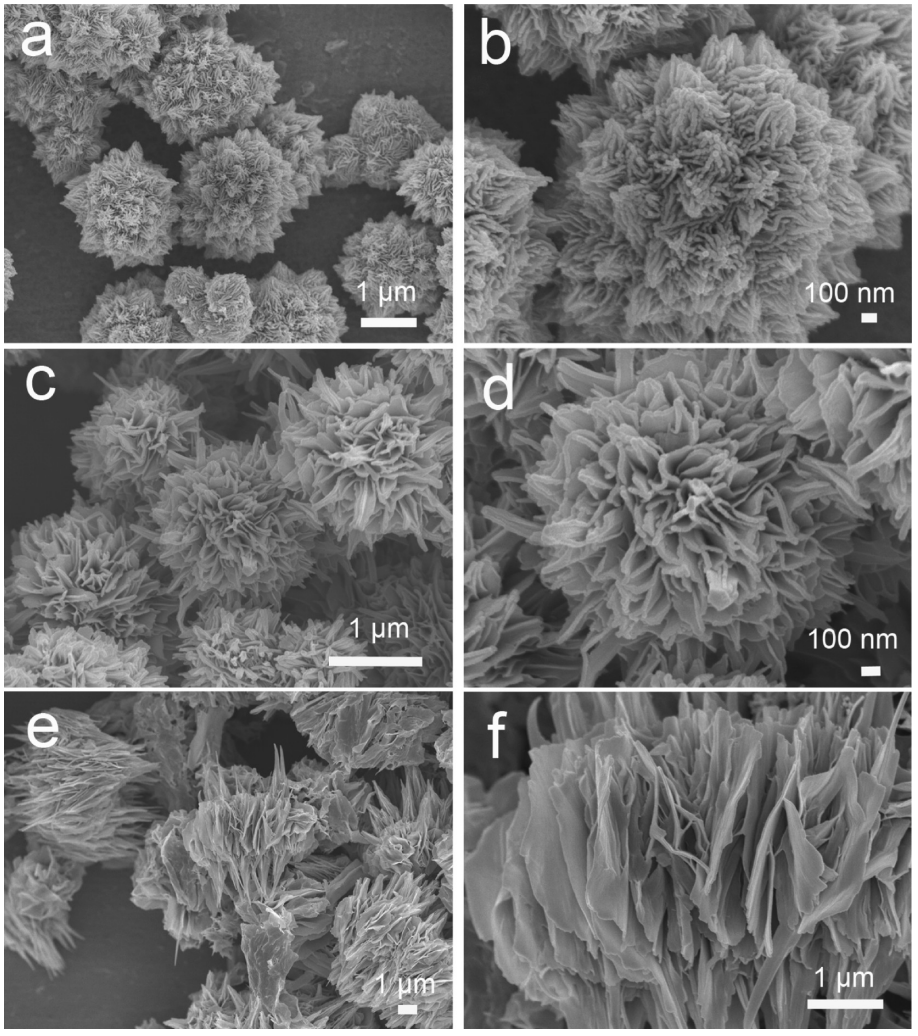

Figure 3. FESEM images of the products prepared by using VOC_2O_4 solutions with different concentrations: (a, b) 0.165 M, (c, d) 0.082 M, and (e, f) 0.055 M.

deionized water under vigorous stirring at 80 °C for several hours until a blue clear solution (VOC_2O_4) is formed. Five mL of such obtained VOC_2O_4 (0.33 M) solution was then added into a 50 mL Teflon container, followed by addition of 1 mL of H_2O_2 (35 wt %) under stirring. After 20 min, 15 mL of ethanol was added and the obtained solution was stirred for another 30 min. Then the container was sealed in an autoclave and transferred to an electrical oven and kept at 170 °C for different durations of 0.5, 2, and 24 h. After cooling down naturally, the precipitates were collected by centrifugation and washed with pure ethanol for three times, then dried at 80 °C overnight. The as-synthesized precipitates with heating durations of 0.5 h, 2 and 24 h were designated as VO-0.5 h, VO-2 h, and VO-24 h, respectively. In order to further study the concentration effect on the morphologies of the products, VOC_2O_4 solutions with the concentration of 0.165, 0.082, and 0.055 M are used without changing other parameters. V_2O_5 urchin-like microflowers were obtained by further calcining VO-2 h and VO-24 h in air at 350 °C for 2 h with a heating rate of 2 °C min^{-1}. The obtained V_2O_5 microflowers are designated as V_2O_5-2 h and V_2O_5-24 h, respectively.

Materials Characterization. Crystallographic phases of all the products were investigated by powder X-ray diffraction (Bruker, D8-Advance XRD, Cu Kα, λ = 1.5406 Å). Morphologies of samples were examined by field-emission scanning electron microscopy (FESEM; JEOL, JEM-2100F) and transmission electron microscopy (TEM; JEM-2010, 200 kV). Measurement of specific surface area and analysis of porosity for the vanadium oxide products were performed through measuring N_2 adsorption−desorption isotherms at 77 K with a Quantachrome Autosorb AS-6B system.

Electrochemical Measurements. The working electrode slurry was prepared by dispersing V_2O_5, carbon black (Super P−Li) and poly-(vinylidene fluoride) (PVDF) binder in an *N*-methylpyrrolidone solution at a weight ratio of 70: 20: 10. The slurry was spread on aluminum foil disks and dried in a vacuum oven at 120 °C overnight prior to Swagelok-type cells assembly. Lithium foil was used as the counter and reference electrode, and 1.0 M $LiPF_6$ in ethyl carbonate/dimethyl carbonate (1:1 v/v ratio) was used as the electrolyte. Cyclic voltammetry measurements were performed on a CHI660C electrochemical workstation. Galvanostatic charging/discharging was conducted on a battery tester (NEWAER).

RESULTS AND DISCUSSION

The time-dependent phase evolution of the solvothermally prepared samples is studied by XRD. As shown in Figure 1, two broad peaks have been observed for the VO-0.5 h sample. The first broad (001) peak is assigned to $V_2O_5{\cdot}nH_2O$,[12] which is formed from the oxidation of VOC_2O_4 by H_2O_2. The material is partially reduced by ethanol after solvothermal treatment for 0.5 h as indicated by the most intensive (110) peak for the monoclinic VO_2 (B) phase.[37] The reduction of V^{5+} by alcohol has been extensively studied,[38] because V_2O_5 has been widely used as a sensor material for ethanol detection.[12,39] It is interesting to find that all the peaks for the VO-2 h sample are in good agreement with the monoclinic VO_2 (B) phase (JCPDS No. 81−2392) with the lattice constants of a = 12.09 Å, b = 3.702 Å, c = 6.433 Å.[37] No other

dx.doi.org/10.1021/am3012593 | ACS Appl. Mater. Interfaces 2012, 4, 3874−3879

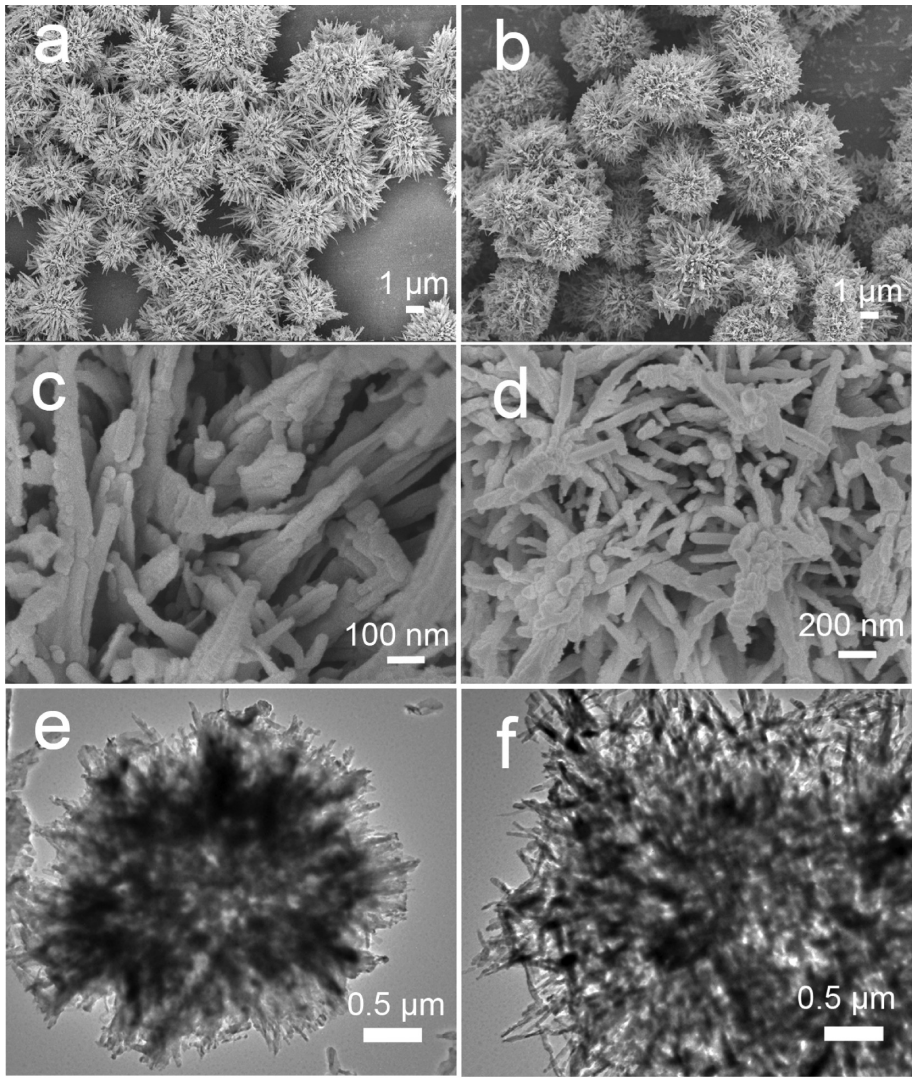

Figure 4. FESEM images of (a, c) V_2O_5-2 h and (b, d) V_2O_5-24 h microflowers obtained from VO-2 h and VO-24 h samples, respectively, by calcination in air at 350 °C for 2 h; the corresponding TEM images of (e) V_2O_5-2 h and (f) V_2O_5-24 h.

phases are observed, which indicates the complete reduction of V_2O_5 xerogel by ethanol. Extending the solvothermal reaction time to 24 h would not cause further phase change, although the intensity of peaks from the VO_2 (B) monoclinic phase increases. The result indicates the facile synthesis of phase-pure VO_2 monoclinic VO_2 phase by this method. After calcination in air at 350 °C for 2 h, the as-synthesized VO_2 can be easily transformed to the V_2O_5 phase as shown in Figure 1. The peaks in the XRD pattern can be perfectly indexed to the orthogonal V_2O_5 phase (JCPDS No. 41−1426; space group *Pmmn* (56), a = 11.516 Å, b = 3.566 Å, c = 3.777 Å).[9,34]

Figure 2 shows the FESEM images of VO-0.5 h, VO-2 h, and VO-24 h samples. As shown in the FESEM images, uniform urchin-like microflowers with an average diameter of about 4 μm are composed of one-dimensional (1D) building blocks for all three samples. As shown in Figure 2a, microflowers are rapidly formed within half an hour in this solvothermal synthesis, which is much more efficient than the literature method.[35] The morphology of the microflowers does not change much with the reaction time (Figure 2c, e). However, the structure and size of the building blocks vary with the solvothermal reaction time. Figure 2b, d, and f are high-magnification FESEM images of VO-0.5 h, VO-2 h, and VO-24 h samples, respectively. As shown in Figure 2b, the 1D building blocks of VO-0.5 h are composed of several nanosheets with the thickness of less than 20 nm. The nanosheet-assembled 1D building blocks can still be observed for the VO-2 h sample as shown in Figure 2d. But for the VO-24 h sample, it is interesting to observe that the building blocks with the overall diameter of around 100 nm are composed of closely stacked nanobelts with a thickness of around 20 nm.

The effect of the VOC_2O_4 concentration on the morphologies of the products has also been investigated. Figure 3a, b show the FESEM images of the product prepared with a concentration of 0.165 M VOC_2O_4. It appears that the exterior surface of vanadium oxide microstructures is composed of nanohorns, which are further assembled from several nanosheets. The diameter of the microstructures is around 1 to 2 μm. When a lower concentration (0.082 M) of VOC_2O_4 is used, 3D hierarchical microflowers with large nanosheets are formed and the thickness of the nanosheets can be less than 20 nm (Figure 3c, d). Further lowering the concentration of VOC_2O_4 to 0.055 M leads to formation of nanosheet-assembled microbundles. As shown in images e and f in Figure 3, the nanosheets are growing along the same direction and the thickness of nanosheets is around 20 nm. To the best of our knowledge, these vanadium oxide microstructures

composed of nanosheets are not reported before. Furthermore, the results show that the present synthesis system is quite versatile. Different 3D hierarchical nano/microstructures, such as urchin-like microflowers, microspheres with nanohorns, microflowers with nanosheets, and nanosheet-bundles can be controllably synthesized by adjusting the concentration of the vanadium precursor solution (VOC_2O_4).

Figure 4 shows the FESEM and TEM images of V_2O_5 microflowers obtained from the VO-2 h and VO-24 h samples by annealing in air at 350 °C for 2 h. The obtained V_2O_5 samples are designated as V_2O_5-2 h and V_2O_5-24 h, respectively. As shown in Figure 3a and b, the urchin-like structures are well preserved after calcination for both of the V_2O_5-2 h and V_2O_5-24 h samples. The FESEM images at a higher magnification (Figure 4c,d) reveal the detailed structures of the nanosized building blocks. The nanobelt structures can still be observed from the building blocks of V_2O_5-2 h microflowers with the thickness ranging from 20 to 50 nm (Figure 4c). However, the building blocks of V_2O_5-24 h microflowers are typically composed of nanorods (Figure 4d). It is believed that the nanorods are produced from the closely stacked nanobelts (see Figure 2f) by thermal sintering. The diameter of the nanorods ranges from 50 to 100 nm. The V_2O_5 microflowers in V_2O_5-2 h and V_2O_5-24 h samples are further investigated by TEM and their structures are shown in Figure 4e and 4f, respectively. Clearly, the microflower structures are composed of nanorods. More importantly, a highly porous texture is revealed by the TEM observation both on the surface of the microflowers and in the interior of the microstructures. The Brunauer–Emmett–Teller (BET) specific surface areas of V_2O_5-2 h and V_2O_5-24 h are measured to be 33.64 and 24.18 $m^2\ g^{-1}$, respectively. These porous structures in electrode materials of LIBs are quite interesting because the kinetics of redox reaction involved can be greatly improved.[40]

The electrochemical properties of the urchin-like V_2O_5-2 h electrode are first evaluated by cyclic voltammetry. Figure 5a shows the first three consecutive cyclic voltammograms (CV) of the V_2O_5-2 h electrode. During the cathodic scan, three peaks at 3.34, 3.14, and 2.2 V (vs Li/Li^+) are clearly observed, which are attributed to the three crystal phase changes of α-V_2O_5 to ε-$Li_{0.5}V_2O_5$, ε-$Li_{0.5}V_2O_5$ to δ-LiV_2O_5 and last δ-LiV_2O_5 to γ-$Li_2V_2O_5$, respectively.[18,29] Also, three corresponding anodic peaks related to the lithium ions removal are observed, which indicates the good reversibility of the electrode materials. Despite the reduced peak intensity, the peak position and the shape of the CV curves are quite similar for consecutive cycles, suggesting the good stability of the electrodes. Figure 5b shows the charge–discharge curves of first, 10th, 20th and 50th cycles for the V_2O_5-2 h electrode at a constant current density of 300 mA g^{-1} between 2 and 4 V vs Li/Li^+. A specific discharge capacity of 274 mA h g^{-1} can be obtained for the V_2O_5-2 h sample in the first cycle. Three typical plateaus at about 3.3, 3.1, and 2.2 V vs Li/Li^+ are clearly observed as more Li^+ ions are intercalated into the structure with three corresponding deintercalation plateaus observed on the charge curves, indicating the high reversibility of the crystal phase changes. These results are in a good agreement with the above CV results. The cycling performance for the V_2O_5-2 h and V_2O_5-24 h electrodes at different current densities and the Coulombic efficiency of the V_2O_5-2 h electrode are shown in Figure 5c. After 50 cycles, specific discharge capacities of 219 and 190 mA h g^{-1} can be retained for V_2O_5-2 h and V_2O_5-24 h electrodes, respectively. And their corresponding capacity fading rates are only 0.4% and 0.5% per cycle. The slightly better capacity retention for the V_2O_5-2 h electrode

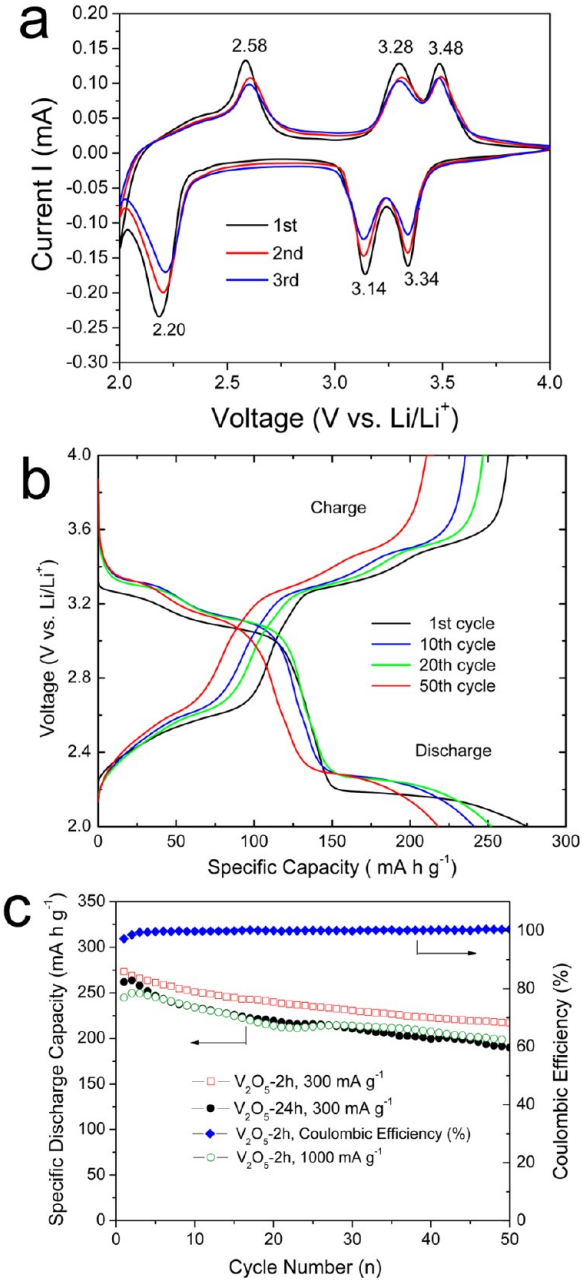

Figure 5. (a) CV curves for the first three cycles of the V_2O_5-2 h electrode at a scan rate of 2 mV s^{-1}; (b) the discharge/charge curves of the 1st, 10th, 20th, and 50th cycles at the current density of 300 mA g^{-1}; (c) cycling performance for V_2O_5-2 h and V_2O_5-24 h and the Coulombic efficiency of the V_2O_5-2 h electrode.

might be attributed to the thinner thickness of the building blocks of V_2O_5-2 h and its higher surface area. The Coulombic efficiency of the V_2O_5-2 h electrode is close to 100% (shown in Figure 5c), suggesting the good reversibility for the Li^+ ion insertion/deinsertion processes. The V_2O_5-2 h is also cycled at a much higher current density of 1000 mA g^{-1} and a specific discharge capacity of 250 mA h g^{-1} can be obtained in the first cycle. Remarkably, the cycling performance is very close to the one at 300 mA g^{-1}, which demonstrates the good rate capability of the V_2O_5-2 h sample. The electrochemical performance of these urchin-like V_2O_5-2 h microstructures is much better than that of previously reported V_2O_5 nanoparticles,[24] nanorods,[25] and nanotubes.[27] It is even better than that of V_2O_5 nanowire/graphene

dx.doi.org/10.1021/am3012593 | ACS Appl. Mater. Interfaces 2012, 4, 3874–3879

composites reported recently.[41] The improved rate capability and cycling stability are attributed to the interesting 3D urchin-like porous structure. More specifically, the porous structure of the microflowers would facilitate the electrolyte penetration and increase the contact area between the electrode material and the electrolyte. Moreover, the nanosized building blocks (i.e., 20−50 nm in thickness for the nanobelts and 50−100 nm in diameter for the nanorods) reduce the distance for Li^+ ions diffusion and the electron transport. Furthermore, the porous structure might be also of advantage to accommodate the volume variations during the Li^+ ions intercalation and deintercalation.

CONCLUSIONS

In summary, 3D hierarchical vanadium oxide microstructures, including urchin-like microflowers, microspheres with nanohorns, nanosheet-assembled microflowers and nanosheet bundles have been successfully synthesized through a solvothermal method without using any surfactants. The morphologies of the microstructures can be easily tailored by varying the concentration of the vanadium oxalate solution. The time-dependent urchin-like microstructures have been studied and their derived V_2O_5 products by calcination have been evaluated as cathode materials for lithium-ion batteries. The obtained V_2O_5 microflowers after calcination well preserve the morphology of the VO_2 microflowers. The as-obtained V_2O_5 microflowers are highly porous with a surface area of 33.64 $m^2\ g^{-1}$. When evaluated as a cathode material for lithium-ion batteries, these urchin-like V_2O_5 microstructures exhibit high lithium storage capacity and enhanced cycling stability and rate capability.

AUTHOR INFORMATION

Corresponding Author

*E-mail: xwlou@ntu.edu.sg.

Notes

The authors declare no competing financial interest.

ACKNOWLEDGMENTS

The authors acknowledge the financial support from Institute of Nanosystems Interface Science and Technology (INSIST) at Nanyang Technological University.

REFERENCES

(1) Armand, M.; Tarascon, J.-M. *Nature* **2008**, *451*, 652.
(2) Winter, M.; Brodd, R. J. *Chem. Rev.* **2004**, *104*, 4245.
(3) Lou, X. W.; Li, C. M.; Archer, L. A. *Adv. Mater.* **2009**, *21*, 2536.
(4) Tarascon, J.-M.; Armand, M. *Nature* **2001**, *414*, 359.
(5) Guo, Y.-G.; Hu, J.-S.; Wan, L.-J. *Adv. Mater.* **2008**, *20*, 2878.
(6) Arico, A. S.; Bruce, P.; Scrosati, B.; Tarascon, J.-M.; Schalkwijk, W. V. *Nat. Mater.* **2005**, *4*, 366.
(7) Zhou, L.; Zhao, D.; Lou, X. W. *Angew. Chem., Int. Ed.* **2012**, *51*, 239.
(8) Sakamoto, J. S.; Dunn, B. *J. Electrochem. Soc.* **2002**, *149*, A26.
(9) Hu, Y.-S.; Liu, X.; Muller, J.-O.; Schlogl, R.; Maier, J.; Su, D. S. *Angew. Chem., Int. Ed.* **2009**, *48*, 210.
(10) Wang, Y.; Cao, G. Z. *Adv. Mater.* **2008**, *20*, 2251.
(11) Washs, I. E. *Catal. Today* **2005**, *100*, 74.
(12) Liu, J.; Wang, X.; Peng, Q.; Li, Y. *Adv. Mater.* **2005**, *17*, 764.
(13) Xiong, C.; Aliev, A. E.; Gnade, B.; Balkus, K. J., Jr. *ACS Nano* **2008**, *2*, 293.
(14) Choi, D.; Blomgren, G. E.; Kumta, P. N. *Adv. Mater.* **2006**, *18*, 1178.
(15) Chen, Z.; Veronica, A.; Wen, J.; Zhang, Y.; Shen, M.; Dunn, B.; Lu, Y. *Adv. Mater.* **2011**, *23*, 791.
(16) Sathiya, M.; Prakash, A. S.; Ramesha, K.; Tarascon, J.-M.; Shukla, A. K. *J. Am. Chem. Soc.* **2011**, *133*, 16291.
(17) Whittingham, M. S.; Song, Y. N.; Lutta, S.; Zavalij, P. Y.; Chernova, N. A. *J. Mater. Chem.* **2005**, *15*, 3362.
(18) Pan, A. Q.; Zhang, J.-G.; Nie, Z. M.; Cao, G. Z.; Arey, B. W.; Li, G. S. *J. Mater. Chem.* **2010**, *20*, 9193.
(19) Kang, K. S.; Meng, Y. S.; Breger, J.; Grey, C. P.; Ceder, G. *Science* **2006**, *311*, 977.
(20) Wang, J.; Sun, X. *Energy Environ. Sci.* **2012**, *5*, 5163.
(21) Ban, C.; Chernova, N. A.; Whittingham, M. S. *Electrochem. Commun.* **2009**, *11*, 522.
(22) Muster, J.; Kim, G. T.; Krstic, V.; Park, J. G.; Park, Y. W.; Roth, S.; Burghard, M. *Adv. Mater.* **2000**, *12*, 420−424.
(23) Watanabe, T.; Ikeda, Y.; Ono, T.; Hibino, M.; Hosoda, M.; Sakai, K.; Kudo, T. *Solid State Ionics* **2002**, *151*, 313.
(24) Ng, S. H.; Patey, T. J.; Buechel, R.; Krumeich, F.; Wang, J. Z.; Liu, H. K.; Pratsinis, S. E. *Phys. Chem. Chem. Phys.* **2009**, *11*, 3748.
(25) Takahashi, K.; Lim, S. J.; Wang, Y.; Cao, G. Z. *Jpn. J. Appl. Phys., Part 1* **2005**, *44*, 662.
(26) Mai, L. Q.; Xu, X.; Xu, L.; Han, C. H.; Luo, Y. *J. Mater. Res.* **2011**, *26*, 2175.
(27) Wang, Y.; Takahashi, K.; Shang, H. M.; Cao, G. Z. *J. Phys. Chem. B* **2005**, *109*, 3085.
(28) Wang, H.; Huang, K.; Huang, C.; Liu, S.; Ren, Y.; Huang, X. *J. Power Sources* **2011**, *196*, 5645.
(29) Zhang, X. F.; Wang, K. X.; Xiao, W.; Chen, J. S. *Chem. Mater.* **2011**, *23*, 5290.
(30) Mai, L. Q.; Xu, L.; Han, C.; Xu, X.; Luo, Y.; Zhao, S.; Zhao, Y. *Nano Lett.* **2010**, *10*, 4750.
(31) Liu, H.; Wang, Y.; Li, H.; Yang, W.; Zhou, H. *ChemPhysChem* **2010**, *11*, 3273.
(32) Wang, S.; Li, S.; Sun, Y.; Feng, X.; Chen, C. *Energy Environ Sci.* **2011**, *4*, 2854.
(33) Liu, P.; Lee, S.-H.; Tracy, C. E.; Yan, Y.; Turner, J. A. *Adv. Mater.* **2002**, *14*, 27.
(34) Cao, A. M.; Hu, J. S.; Liang, H. P.; Wan, L. J. *Angew. Chem., Int. Ed.* **2005**, *44*, 4391.
(35) Dwyer, C. O.; Navas, D.; Lavayen, V.; Benavente, E.; Ana, M. A. S.; Gonzalez, G.; Newcomb, S. B.; Torres, C. M.S. *Chem. Mater.* **2006**, *18*, 3016.
(36) Zhong, L. S.; Hu, J. S.; Liang, H. P.; Cao, A. M.; Song, W. G.; Wan, L. J. *Adv. Mater.* **2006**, *18*, 2426.
(37) Huang, J.; Wang, X.; Liu, J.; Sun, X.; Wang, L.; He, X. *Int. J. Electrochem. Sci.* **2011**, *6*, 1709.
(38) Rahman, M. M.; Wang, J. Z.; Idris, N. H.; Chen, Z.; Liu, H. *Electrochim. Acta* **2010**, *56*, 693.
(39) Biette, L.; Carn, F.; Maugey, M.; Achard, M. F.; Maquet, J.; Steunou, N.; Livage, J.; Serier, H.; Backov, R. *Adv. Mater.* **2005**, *17*, 2970.
(40) Lou, X. W.; Deng, D.; Lee, J. Y.; Archer, L. A. *Chem. Mater.* **2008**, *20*, 6562.
(41) Liu, H.; Yang, W. *Energy Environ. Sci.* **2011**, *4*, 4000.